

**Origin of Dual Emission in σ Bridged Donor-Acceptor TADF Compounds**

Journal:	<i>Journal of Materials Chemistry C</i>
Manuscript ID	TC-ART-07-2019-003548.R1
Article Type:	Paper
Date Submitted by the Author:	17-Sep-2019
Complete List of Authors:	Skaisgiris, Rokas ; Vilnius University, Institute of Photonics and Nanotechnology Serevičius, Tomas; Vilnius University, Institute of Photonics and Nanotechnology Kazlauskas, Karolis; Vilnius University, Institute of Photonics and Nanotechnology Geng, Yan; Shandong Normal University, College of Chemistry, Chemical Engineering and Materials Science Adachi, Chihaya; Kyushu University, Center for Organic Photonics and Electronics Research (OPERA) Jursenas, Saulius; Vilnius University, Institute of Photonics and Nanotechnology

Origin of Dual Emission in σ Bridged Donor-Acceptor TADF Compounds

Rokas Skaisgiris¹, Tomas Serevičius^{1,*}, Karolis Kazlauskas¹, Yan Geng⁴, Chihaya Adachi^{2,3*} and Saulius Juršėnas¹

¹Institute of Photonics and Nanotechnology, Vilnius University, Sauletekio 3, LT-10257, Vilnius, Lithuania

²Center for Organic Photonics and Electronics Research (OPERA), and International Institute for Carbon Neutral Energy Research (WPI-I²CNER), Kyushu University, Fukuoka 819-0395, Japan.

³Japan Science and Technology Agency ERATO, Adachi Molecular Exciton Engineering Project, Fukuoka 819-0395, Japan

⁴College of Chemistry, Chemical Engineering and Materials Science, Collaborative Innovation Center of Functionalized Probes for Chemical Imaging in Universities of Shandong, Key Laboratory of Molecular and Nano Probes, Ministry of Education, Shandong Normal University, Jinan 250014, P. R. China

*Corresponding authors: tomas.serevicius@tmi.vu.lt, adachi@cstf.kyushu-u.ac.jp

Abstract

The desire to boost the reverse intersystem crossing rate and obtain thermally activated delayed fluorescence with sub-microsecond lifetime fosters the search of novel concepts of molecular geometry. Recently, TADF compounds made of acridine, tetramethylcarbazole and triphenylamine donor and triphenyltriazine acceptor units bound by hyperconjugated spacer unit were introduced as having very rapid double TADF decay. Here we present an in-depth time-resolved fluorescence analysis of these intriguing donor- σ -acceptor TADF compounds in various surroundings. Extremely weak coupling of electron-donating and electron-accepting units was found for the σ -bridged TADF compounds, resulting in the coexistence of intramolecular and exciplex fluorescence, which interplay allowed to tune the emission properties. The initial fluorescence decay in toluene solutions, previously attributed to rapid TADF, was shown to be the prompt intramolecular fluorescence with prolonged fluorescence lifetime, susceptible to molecular oxygen. Only the later delayed fluorescence at the microsecond time-scale, originating from the exciplex states, was attributed to TADF. On the contrary, the dominant intramolecular TADF was observed in diluted PMMA films with weaker non-radiative decay. The smooth transition from intramolecular to exciplex TADF was observed by increasing the doping concentration of polymer films. DF/PF ratio was found to increase with the increasing doping concentration due to emergence of additional exciplex TADF until the 20 wt% doping load, when the concentration quenching emerged at the larger doping ratios. The presented findings showcase the unusual fluorescence properties of TADF compounds with weakly bound donor and acceptor units and are important for the future design of novel TADF compounds.

Introduction

Organic light emitting diodes (OLEDs) are highly attractive for lighting and display applications due to unmatched contrast ratio, lightness and flexibility. The long history of OLED science, dating back to the report by Tang and Van Slyke¹, mostly was devoted to the improvement of external quantum efficiency (EQE), which was limited by the dark triplet states. Singlet exciton yield of electrically injected charge carriers for the 1st generation fluorescent OLEDs is only 25%, limiting its external quantum efficiency (EQE) for up to about 5%. Later, a new class of phosphorescent emitters, employing internal heavy atom effect was introduced². The involvement of heavy rear-earth atoms, e.g., iridium, resulted in the remarkable enhancement of the spin-orbit coupling, converting all excitons to short-lived triplet ones. This strategy allowed to reach 100% internal quantum efficiency (IQE) and EQE of 20% for phosphorescent OLEDs³. However, phosphorescent compounds, especially the blue emitters, suffered from instability. Moreover, the requirement of rear-earth metals increased the cost of the device and raised the concerns for their toxicity. Stability and high-cost issues were solved by introducing the 3rd generation all-organic emitters employing thermally activated delayed fluorescence^{4,5}. In this case, molecular compounds are designed to have low singlet-triplet energy splitting (ΔE_{ST}) when the triplet excitons are thermally assisted to perform reverse intersystem crossing with internal quantum efficiencies up to 100%^{6,7}. Several different approaches for the realization of low ΔE_{ST} were suggested: minimization of the exchange interaction by using donor-acceptor molecular compounds⁵, utilization of multiple resonance effect⁸ or by employing the excited-states^{9,10}. Yet, the donor-acceptor core still is the mostly used TADF design. In this case an efficient reverse intersystem crossing (rISC) is achieved by minimizing the exchange energy (J), which is directly proportional to HOMO-LUMO overlap¹¹ and ensuring strong vibronic coupling between the localized (³LE) and charge-transfer (³CT) triplet states^{12,13}. The low HOMO-LUMO overlap is attained in compounds constructed of electron-donating (D) and electron-accepting (A) molecular fragments with balanced steric hindrance, having pronounced charge-transfer (CT) character and non-negligible radiative recombination rate.

The same concept based on the minimization of ΔE_{ST} by reducing the HOMO-LUMO overlap was utilized in exciplex emitters^{14,15}, composed of electron-donating and electron-accepting molecular materials. Though the low ΔE_{ST} in exciplex systems can be realized more easily due to intermolecular nature of charge transfer and rather efficient exciplex-based OLEDs with EQE approaching 20% have been presented¹⁶, the efficiency of exciplex TADF highly depends on the distance between donor and acceptor fragments¹⁷ which is difficult to control. This strongly complicates the applications of exciplex TADF OLEDs. To overcome the shortcomings of exciplex TADF, a novel strategy was suggested. In this case donor and acceptor units were bound in a close proximity (e.g. several Å) with the conjugated¹⁸ or non-conjugated^{19–22} spacers utilizing

intermolecular through-space charge transfer. Rather efficient exciplex TADF can be achieved with the fluorescence quantum efficiencies (Φ_F) up to about 60% and EQE up to about 12%. Another promising pathway for similar “fixed” exciplex systems is to employ hyperconjugation^{23,24}, which allows to bound two separated π -conjugated electron systems. Recently, we have suggested a novel donor- σ -acceptor geometry utilizing hyperconjugation effect to obtain TADF²⁵. Several donor units were bound to triphenyltriazine acceptor fragment by hexafluoroisopropylidene spacer unit. In this case, the hyperconjugation between the donor and acceptor moieties ensured very low HOMO-LUMO overlap, low ΔE_{ST} together with the intramolecular nature of CT. DFT-estimated oscillator strengths were very low (in the range of 0.0008 – 0.0054), typical for weakly interacting donor and acceptor systems. Dual TADF decay was observed, one of which was very rapid with lifetime of only 200-400 ns which is one of the lowest ever reported²⁶. Successful realization of TADF with sub-microsecond lifetime in similar hyperconjugation-based compounds could open new possibilities for realization of highly efficient OLEDs with low roll-off²⁷.

Inspired by the intriguing TADF properties of donor- σ -acceptor TADF compounds with sub-microsecond lifetime²⁵, here we performed the comprehensive time-resolved fluorescence study of σ bridged TADF compounds with dual upconversion in various surroundings. Analysis of viscosity, concentration and temperature-dependent fluorescence spectra of TADF compounds in dilute solutions, dilute polymer and neat films revealed the interplay of two different CT states, decaying on different time-scales. Molecular concentration and ambient viscosity was shown to tune the emission type, intramolecular or intermolecular CT or even from both types simultaneously. Intramolecular TADF was observed only in diluted polymer films, while the coexisting exciplex emission was shown to be of TADF nature in solutions and films at high doping concentration.

1. Experimental details

Photophysical properties were measured in 1.2×10^{-5} M toluene solutions, PMMA (poly(methylmethacrylate)) films with variable doping concentration (1 – 100 wt %) and neat films. The analysis of 1CT_2 state was also performed in 1×10^{-4} M toluene solutions. The PMMA films were prepared by dissolving compound and PMMA at appropriate rations in toluene and then drop-casting at room temperature on a quartz substrate. Neat films were prepared from 5 mg/ml toluene solution by spin-coating at 800 rpm for 1 min and finalizing with 8 min of 4000 rpm to accelerate the evaporation of toluene. To modify the viscosity of toluene, PMMA polymer was added into solution in different proportions²⁸. The absorption spectra were measured by UV-Vis-NIR spectrophotometer Lambda 950 (Perkin Elmer). Steady-state emission spectra were recorded by CCD spectrometer PMA-11 (Hamamatsu) coupled with a CW xenon lamp (FWHM < 10 nm). Fluorescence quantum yields (Φ_F) were obtained by using the integrating sphere method²⁹. Time-resolved fluorescence

spectra, fluorescence decay transients and phosphorescence spectra were obtained by using nanosecond YAG:Nd³⁺ laser NT 242 with optical parametric generator (Ekspla, excitation wavelength 300 nm, pulse duration 7 ns, repetition rate 1 kHz, 50 nJ/pulse fluence) and time-gated intensified CCD camera iStar DH340T (Andor) with spectrograph SR-303i (Shamrock). Phosphorescence spectra were measured at 10 K temperature after 100 μ s delay with 890 μ s integration time. Fluorescence decay transient measurements were performed by exponentially increasing delay and integration time as described in ref.³⁰ This allowed to record up to 10 orders of magnitude in time and intensity of the photoluminescence decay. Five repetitive freeze–pump–thaw cycles were used to deoxygenate toluene solutions. Polymer samples were mounted in closed cycle He cryostat (Cryo Industries 204N) for both oxygen-saturated and oxygen-free (at 1×10^{-4} Torr pressure) measurements. Temperature dependent measurements were performed in the same closed cycle He cryostat.

Results and Discussion

Materials and steady-state spectroscopy analysis of diluted solutions

Three TADF compounds of donor- σ -acceptor structure were analyzed. Planar triphenyltriazine fragment was used as an electron-acceptor unit while dihydroacridine (**1**), tetramethylcarbazole (**2**) and triphenylamine (**3**) were selected as electron-donating units with different electron-donating strengths³¹. Hexafluoroisopropylidene was used as a σ -spacer. Synthetic details, initial DFT calculations and brief analysis of fluorescence properties were reported elsewhere²⁵ and is briefly reported in this chapter, while the thorough spectroscopic analysis will be presented in the following chapters.

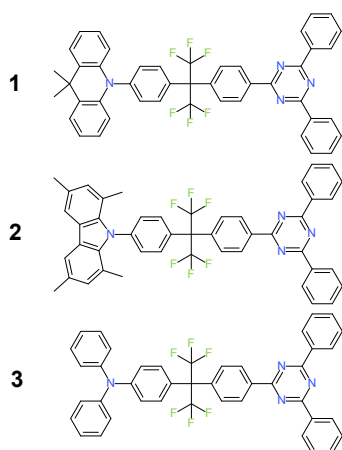


Fig. 1 Chemical structures of donor- σ -acceptor compounds 1-3.

Absorption spectra peaked below 300 nm with weak absorption of intramolecular charge transfer (ICT) origin at about 300-370 nm, observed for all compounds, in-line with the DFT predictions²⁵. Negligible oscillator strengths of 0.0008, 0.0012 and 0.0054 were simulated for

compounds **1-3**, respectively. Fluorescence spectra of toluene solutions peaked in the range of 437 – 463 nm. Broad and structureless spectral lineshape indicated its charge-transfer nature. Locally excited (^1LE) state emission at about 360 nm was clearly observed for compound **2**, originating from tetramethylcarbazole donor unit²⁵, while for the rest of compounds ^1LE intensity was lower. Low-temperature phosphorescence spectra of toluene solutions (LTPH) were of ^3LE nature with the lowest energy vibronic replicas peaking at 415-419 nm. Singlet-triplet energy gaps (ΔE_{ST}) of 0.06, 0.07 and 0.18 eV were estimated for compounds **1**, **2** and **3**, respectively²⁵.

Excited state relaxation in diluted solutions

Fluorescence decay transients of donor- σ -acceptor compounds **1-3** at CT emission peak in oxygen-free ($-\text{O}_2$) toluene followed double-exponential decay (see Fig. 2). Initially, fluorescence decayed with lifetime of 37-470 ns (τ_{FL1}), followed by the later slower decay with lifetime (τ_{FL2}) of 0.45-10 μs (see Table 1 for details). The presence of oxygen strongly quenched both CT fluorescence bands. Both fluorescence decays in $-\text{O}_2$ toluene, the fast and the slower one, was attributed to TADF in the initial analysis²⁵. Fluorescence quenching by oxygen and TADF intensity activation by temperature were used as the proof. However, the nature of both decays is more complex.

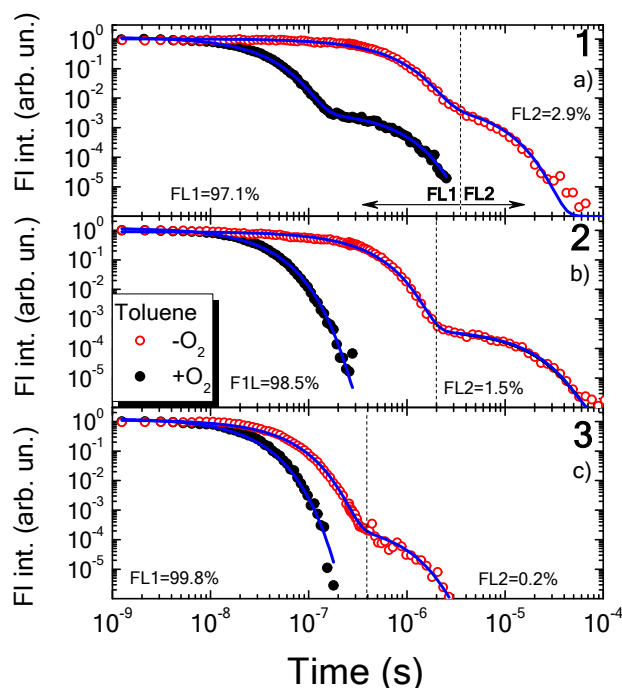


Fig. 2 Normalized fluorescence decay transients of donor- σ -acceptor compounds **1** (a), **2** (b) and **3** (c) in oxygen-saturated ($+\text{O}_2$) and oxygen-free ($-\text{O}_2$) toluene solutions. Fractional intensities of initial and delayed fluorescence in $-\text{O}_2$ conditions are also noted.

The initial decay with lifetime of 37 – 470 ns could also be of prompt fluorescence. This could not be surprising for weakly coupled D- σ -A compounds with low HOMO-LUMO overlap and negligible oscillator strengths. The lowest oscillator strength was estimated for compound **1** with the

largest τ_{FL1} while the lowest – for compound **3** with the largest oscillator strength. ΔE_{ST} and TADF lifetime also depends on the HOMO-LUMO overlap¹¹ (thus the oscillator strength) and more rapid TADF decay should be observed for compounds with smaller ΔE_{ST} . The lowest singlet-triplet energy gap was estimated for compounds **1** and **2** (60 and 70 meV, respectively), while for compound **3** it was remarkably larger (180 meV). However, an opposite trend was observed. As we can see, τ_{FL1} was the longest for compound with the lowest ΔE_{ST} and it was the shortest for compound with the largest ΔE_{ST} . Such trend is on the opposite of what we could expect for TADF, but in-line with the trend for prompt fluorescence: the longest τ_{FL1} was observed for compound **1** with the strongest dihydroacridine donor unit^{25,31} and the lowest oscillator strength, while the shortest τ_{FL1} was observed for compound **3** with the weakest triphenylamine donor unit and the largest oscillator strength. This prompt fluorescence was shown to be susceptible to molecular oxygen. This is rather unusual, however singlet states has been shown to be sensitive to molecular oxygen^{32–34}. Our donor- σ -acceptor compounds with especially long prompt fluorescence lifetime could be even more prone to the quenching by molecular oxygen.

Table 1 Fluorescence data of donor- σ -acceptor compounds **1-3** in oxygen-free toluene

	τ_{FL} (ns) ^a	τ_{TADF} (μs) ^c	DF/PF ^d
1	470	4.5	0.03
2	250	10	0.015
3	37	0.45	0.002

^a Fluorescence decay time of initial fluorescence.

^b Fluorescence decay time of delayed fluorescence

^c Time-integrated delayed and prompt fluorescence intensity ratio.

To analyze the nature of the initial fluorescence, temperature-dependent measurements of fluorescence transients were performed in dilute toluene (see Figs. S6 and S7 in ref.²⁵) and the decrease of τ_{FL1} was observed at larger temperatures, typically for TADF. However, when the compounds were embedded into PMMA polymer films (see Fig. 3), the lifetime and the intensity of the initial decay was insensitive to the temperature. Toluene has melting point of 178 K, therefore it remained in liquid state in the temperature range of 300-200 K, therefore the variation of the non-radiative recombination rate upon the temperature decrease was not neglected. The impact of non-radiative decay was strongly suppressed in rigid polymer film, when no thermal activation were be observed, typically for prompt fluorescence.

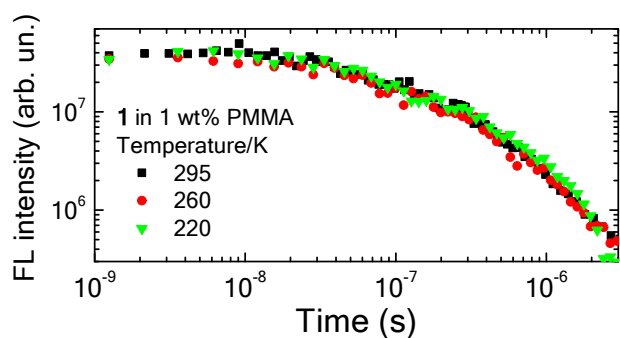


Fig. 3 Initial fluorescence decay transients of 1wt% PMMA films of compounds **1-3**.

The decay time of the later fluorescence, observed at microsecond time-scale, was 4.5, 10 and 0.45 μs (an approximate value due to the low emission intensity) for compounds **1**, **2** and **3**, respectively. In this case, the second decay component followed the TADF-like behavior: its lifetime was lower for compounds with lower ΔE_{ST} and the DF/PF ratio was larger for compounds with lower ΔE_{ST} (see Table 1).

To conclude, the initial fluorescence decay could hardly be attributed to TADF. The experimental evidences show its non-TADF nature. Only the later fluorescence, observed at the microsecond time-scale, can be attributed to TADF.

Two charge-transfer states in dilute solutions

Time-integrated fluorescence spectra (TIFL) of compounds **1-3** in toluene²⁵ showed only one dominating CT fluorescence band with double-exponential decay profile. On the contrary, time-resolved fluorescence spectra (TRFL) analysis (see Fig. 4) revealed the presence of more complex structure of emission spectra. Two CT fluorescence spectra were observed at the different time-scale. Initially, the first CT fluorescence band ($^1\text{CT}_1$) was observed at about 445 – 465 nm up to about 4 μs , 2 μs and 0.5 μs for compounds **1-3**, respectively. At the later delays, the second CT fluorescence band ($^1\text{CT}_2$) clearly emerged peaking at about 475 – 505 nm (see Fig. S1 in ESI). Some long-wavelength shoulder of fluorescence spectra, extending up to 600-650 nm was observed for all compounds even at the lowest delay times, showing that the weak second CT state probably is formed after the photoexcitation, but is overwhelmed by fluorescence of the $^1\text{CT}_1$ state. $^1\text{CT}_2$ emission was more susceptible to oxygen quenching than that of $^1\text{CT}_1$ states (see Fig. S2 in ESI). Since the prompt and delayed fluorescence are observed at different wavelengths, the true TADF transients at the larger delays are those obtained at the $^1\text{CT}_2$ peak (see Fig. S3 in in ESI). An enhanced TADF intensity was observed (up to about 5-6 times) with the same lifetime.

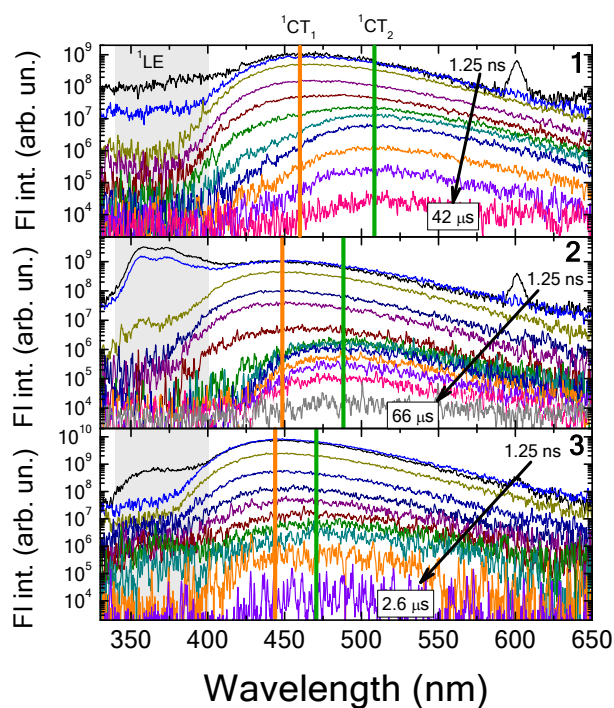


Fig. 4 Time-resolved fluorescence spectra of donor- σ -acceptor compounds **1-3** in oxygen-free toluene. Numbers in picture denotes initial and final delay times.

The nature of both CT states needs further analysis. Clearly, both emission bands are of CT-nature and their peak energies depends on the strength of donor unit: stronger the donor, the more redshifted the emission wavelength. The energy difference between the CT bands was 240, 220 and 160 meV for compounds **1-3**, respectively. The second emission band, which clearly emerges only at the later delays, could originate from, e.g., dynamic molecular conformer states, emerged after the reorganization of molecular structure³⁵ or exciplex states³⁶, formed between the donor and acceptor units from separate molecules after diffusion at long time-scale.

To test the nature of the second CT state, fluorescence decay transients of compound **1** were measured in O_2 toluene solutions with adjustable viscosity (see Fig. 5 and experimental section for the details). More viscous toluene surrounding had weak effect on the prompt emission, slightly decreasing its decay time from 470 to 280 ns, while the increased viscosity strongly quenched TADF when the DF/PF ratio decreased from 0.15 to 0.003 (see Table 2). The decrease of prompt fluorescence lifetime could be related with the changes of non-radiative decay rate. It is clear, that TADF intensity is weakened in viscous surrounding, however still it is not clear, whether the quenching of delayed emission was due to the impeded reorganization of molecular structure or slowed molecular diffusion and thus the lower contribution from exciplex states.

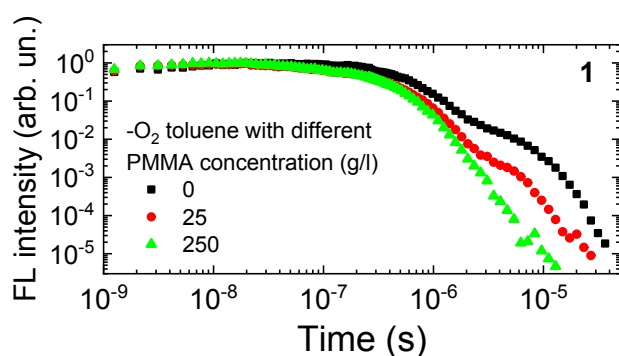


Fig. 5 Fluorescence decay transients of compound **1** at $^1\text{CT}_2$ peak in oxygen-free toluene solutions with different viscosity. Solution viscosity was varied by increasing PMMA concentration²⁸.

Table 2 Photoluminescence decay constants of compound **1** at $^1\text{CT}_2$ peak in toluene with different viscosity.

PMMA concentration (g/l) ^a	DF/PF ratio ^b	$\tau_{1\text{CT}_1}$ (ns) ^c	$\tau_{1\text{CT}_2}$ (μs) ^d
0	0.18	470	4.5
25	0.03	320	2.8
250	0.003	280	1.25

^a PMMA polymer concentration in oxygen-free toluene.

^b Intensity ratio between time-integrated delayed and prompt fluorescence spectra.

^c Fluorescence decay time of CT_1 state (prompt fluorescence).

^d Fluorescence decay time of CT_2 state (TADF).

The presence of exciplex states was revealed by comparing TADF properties of 1.2×10^{-5} and 1×10^{-4} M toluene solutions of compound **1** (see Fig. 6). The lineshape of fluorescence spectra clearly was concentration dependent (see Fig. 6 a), when the emission peak was redshifted from 475 nm to 485 nm upon the concentration increase. As we know from the analysis of time-resolved fluorescence spectra (see Fig. 4), the time-integrated emission spectrum is formed of two distinct fluorescence bands of CT_1 and CT_2 states, peaking at about 465 nm and 505 nm (for compound **1**). Increasing the concentration of compound **1** in toluene clearly enhances the emission intensity from $^1\text{CT}_2$ states and, therefore, shifts the peak of total emission spectrum to the longer wavelengths. The similar trend was observed for fluorescence decay transients, obtained at $^1\text{CT}_2$ emission peak (see Fig. 6 b). Here we can see, that the increased concentration of compound **1** in toluene solutions enlarged the intensity of the later decay part, attributed to exciplex TADF, increasing DF/PF ratio from 0.18 to 0.49.

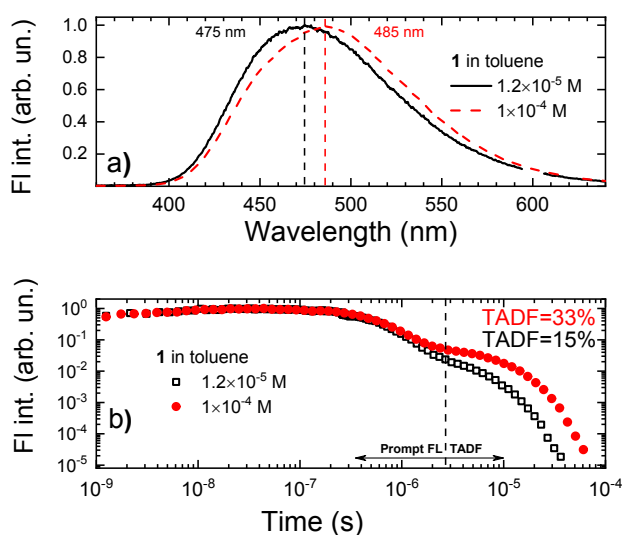


Fig. 6 a) Normalized time-integrated fluorescence spectra of compound **1** in 1.2×10^{-5} M (solid line) and 10^{-4} M (dashed line) oxygen-free toluene solutions. b) Fluorescence decay transients of compound **1** in 1.2×10^{-5} M (open symbols) and 10^{-4} M (closed symbols) oxygen-free toluene solutions at ${}^1\text{CT}_2$ peak.

Clearly, viscosity and concentration-dependent measurements of fluorescence spectra supports the prediction that the second CT state is of exciplex nature. It may look quite unusual to observe exciplex emission in solutions with concentration as low as 1×10^{-5} M, however the exciplex emission can be successfully observed in various diluted solutions of molecular compounds, especially for those containing large and planar units^{37–40}, as in our σ -bonded D-A compounds. Additionally, exceptionally slow fluorescence decay should be beneficiary for the observation of exciplex emission in solutions, when the probability of two molecules to meet each other before the recombination is greatly enhanced. Obviously, the most intense intermolecular TADF was observed for compound with the longest intramolecular fluorescence lifetime (see Fig. 2).

Suppression of the exciplex states in polymer films

For the further analysis of exciplex formation, compounds **1-3** were incorporated into rigid PMMA polymer matrix at low concentration. In this case, emission should originate only from isolated molecules, molecular diffusion is strongly impeded by the rigid polymer ambient. Time-integrated fluorescence spectra of 1 wt% PMMA films of compounds **1-3** are shown in Fig. 7 a. Emission spectra were very similar to those of dilute solutions, showing the dominating intramolecular CT emission peaking at 460, 455 and 445 nm for compounds **1-3**, respectively. Weak emission, related with the electron-donating unit, was clearly observed for compound **2**.

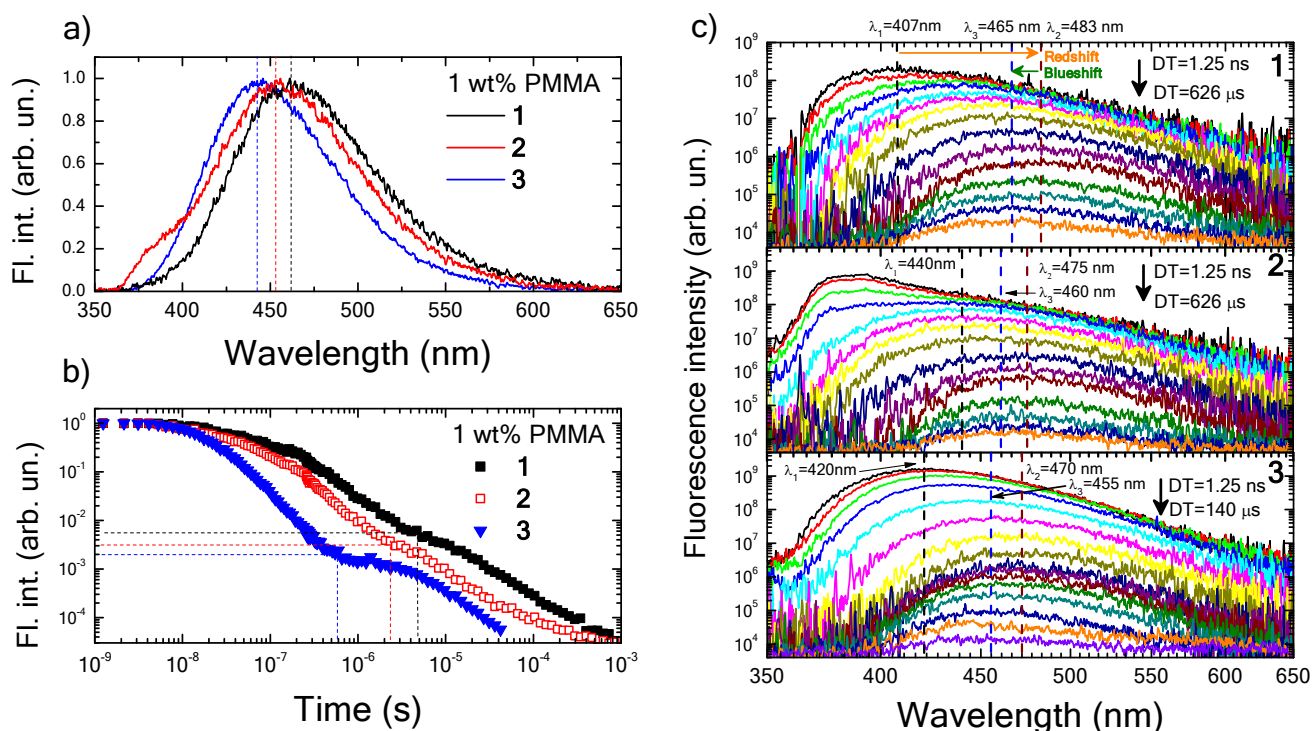


Fig. 7 a) Normalized time-integrated fluorescence spectra of 1 wt% PMMA films of donor- σ -acceptor compounds **1-3**. Dashed lines are guides for eyes. b) Normalized fluorescence decay transients of 1 wt% PMMA films of donor- σ -acceptor compounds **1-3** in in $-O_2$ conditions. Dashed lines denotes the initial intensity of delayed emission and delay time when the delayed emission emerges. c) Time-resolved fluorescence spectra of 1 wt% PMMA films of donor- σ -acceptor compounds **1-3** in $-O_2$ conditions. DT denotes the initial and the latest delay times. λ_1 , λ_2 and λ_3 represent emission peak wavelengths of initial, the most redshifted and the latest emission spectra, respectively.

Fluorescence decay transients of 1 wt% PMMA films of compounds **1-3** are shown in Fig. 7 b. Fluorescence decay followed the same trend as in toluene solutions, when two decay components were observed (see Fig. S4 in ESI). However, fluorescence decay profiles were multiexponential, indicating the existence conformational disorder, typical for TADF compounds⁴¹⁻⁴⁴. Although the exact lifetime of prompt and delayed emission could not be evaluated due to the multiexponential nature, it is clear, that the prompt fluorescence showed the same trend as in toluene solutions, when the slowest prompt fluorescence decay was observed for compound **1** and the most rapid – for compound **3**. For delayed emission, no clear trend was observed. The delayed fluorescence was quenched by oxygen (see Fig. S5 in ESI), typically for TADF. Temperature-dependent fluorescence decay transient measurements also supported our assumptions (see Fig. S6 in in ESI). The intensity of initial fluorescence and its lifetime was insensitive to temperature. On the other hand, the delayed emission showed temperature activation, typically for TADF. TADF intensity was remarkably enhanced in polymer film, when the DF/PF ratios increased up to 1.08, 0.92 and 0.6 for compounds **1**, **2** and **3**, respectively. This was resulted by the lowered non-radiative decay in more rigid surrounding and due to the presence of conformational disorder⁴³.

The analysis of time-resolved fluorescence spectra of compounds **1-3** embedded in 1 wt% PMMA films (see Fig. 7 c) revealed the presence of the temporal shifts of emission peak due to the

dispersion of ΔE_{ST} , typical for TADF in solid surrounding^{41–44}. Initially, the redshift of CT₁ state of about 210–480 meV was observed for about 0.5–4 μ s, while at the later delays the blueshift emerged. The blueshift was comparable for all compounds (\sim 100 meV), while the lowest redshift was observed for compound **2** with sterically-fixed tetramethylcarbazole donor unit. As it was expected, the ¹CT₂ state was totally suppressed in polymer films, again confirming its exciplex nature. Both fluorescence decay components, prompt and delayed, originated from the intramolecular ¹CT₁ state. The non-radiative decay, especially through the internal conversion, is remarkably weakened in rigid polymer ambient, allowing to observe the delayed emission from the intramolecular states.

Exciplex states in neat films

At the final stage, the emission properties of neat films of donor- σ -acceptor compounds **1–3** were analyzed (see Fig. 8).

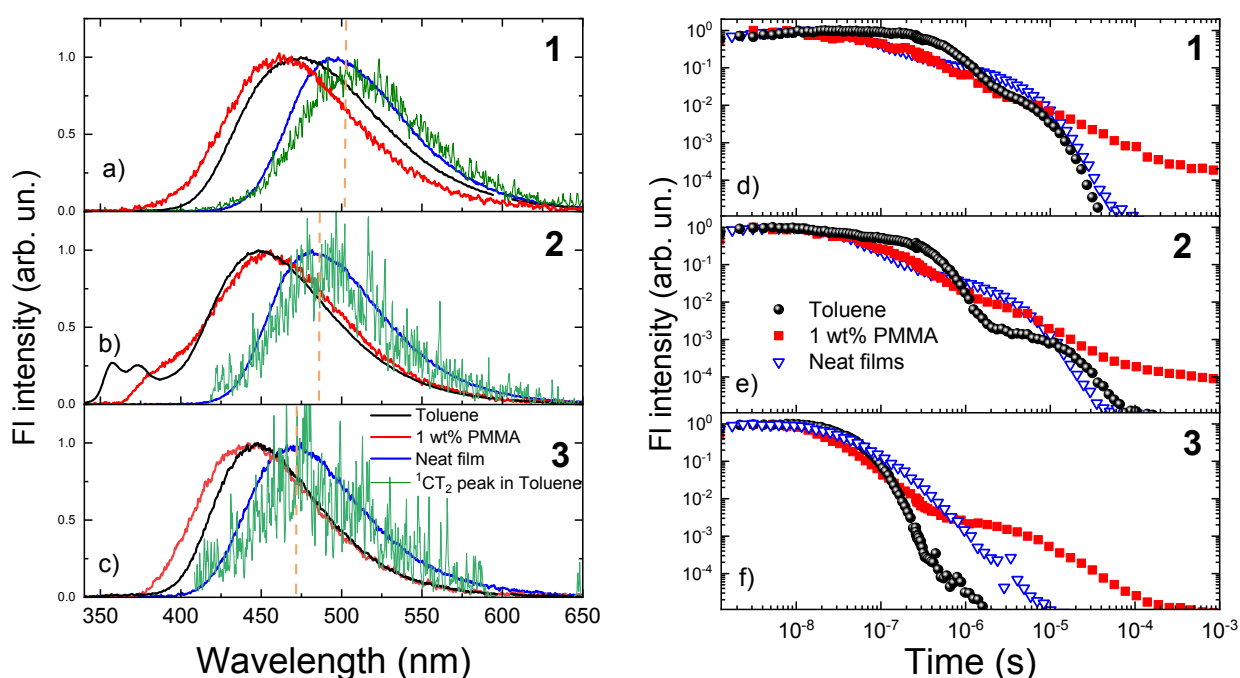


Fig 8 a), b) and c) Normalized time-integrated fluorescence spectra of 1 wt% PMMA films (red lines), 1.2×10^{-5} M toluene solutions (black lines) and neat films (blue lines) together with fluorescence spectra of ¹CT₂ state in toluene solution of donor- σ -acceptor compounds **1–3** in oxygen-free conditions. Vertical lines are guides for eyes. d), e) and f) Normalized fluorescence decay transients of 1 wt% PMMA films (red figures), 1.2×10^{-5} M toluene solutions (black figures) and neat films (blue figures) of donor- σ -acceptor compounds **1–3** in oxygen-free conditions.

As we can see from the Fig. 8 a, time-integrated fluorescence spectra of the neat films of compounds **1–3** were redshifted for about 140–190 meV in respect of 1 wt% PMMA films and 180–200 meV in respect of 1.2×10^{-5} M toluene solutions and peaked at 495, 482 and 470 nm for compounds **1**, **2** and **3**, respectively. The redshift of emission wavelength in neat films is rather frequent effect for both fluorescent and TADF emitters^{45,46} and usually occurs due to the intermolecular interactions or solid state solvation. However, solid state solvation occurs with smaller magnitude due to lower rotation ability of molecules and almost exclusively only after the inclusion

of additional dopants with large ground-state dipole moment^{42,47,48}. Usually the shift of emission peak with increasing doping concentration occurs due to the enhanced intermolecular interactions^{45,49}. In our case, the TIFL spectra of neat films of compounds **1-3** were found to coincide quite well with the fluorescence spectra of ¹CT₂ state from toluene solutions (see blue and green lines in Fig. 8 a), attributed to the emission of exciplex states. Weak exciplex emission, observed in toluene solution, dominated in the neat films. This is not surprising, since the formation of excimer states should be enforced in tightly-packed molecular environment of neat films^{24,50}. Low-temperature phosphorescence spectra of compounds **1-3** were of different nature. If LTPh spectra in toluene contained clear vibronic progression, typical for ³LE states (see Fig. 2 in ref.²⁵), LTPh spectra of neat films were structureless, indicating its intermolecular CT nature²⁴ (see Fig. S7 in ESI). ΔE_{ST} of 60 and 90 meV was estimated for compounds **2** and **3**, respectively. Surprisingly, the negative ΔE_{ST} of -40 meV was estimated for **1**, probably due to the impact of the remaining phosphorescence from the intramolecular states.

Time-resolved fluorescence spectra of neat films of compounds **1-3** are shown in Fig. S8 in ESI. The presence of conformational disorder was observed. Initially, the redshift of emission spectra from about 460 nm to 490 – 510 nm was observed. No subsequent blueshift of emission peak was observed, probably due to the quenching of the latest delayed emission at the defect sites⁴³. Fluorescence decay transients of neat films of compounds **1-3** at ¹CT₂ peak are shown in Fig. 8 d-f, along with emission decay transients of 1.2×10⁻⁵ M toluene solutions and 1 wt% PMMA films. Double-multiexponential decay was observed, when the initial decay of prompt fluorescence reassembled that of 1 wt% PMMA films, while the later decay was rather similar to that of toluene solutions (except the compound **3**). For compound **3**, no clear TADF were observed. As we have already seen, the initial prompt fluorescence was strongly perturbed by conformational disorder, thus its decay was very similar to that of 1 wt% PMMA films. The later TADF emerged only from the lowest-energy conformer states, when the higher-energy emission was quenched, therefore the TADF decay in neat films was less perturbed by the conformational disorder and more similar to that in toluene solutions. The fractional TADF intensity was remarkably enhanced in the neat films (except the compound **3**) due to the larger number of TADF-active exciplex states. The DF/PF ratio for neat films was 1.63 and 1.44 for compounds **1** and **2**, respectively.

The delayed fluorescence of neat films of compounds **1** and **2** showed strong activation by temperature (see Fig. S9 in Supporting Information), typically for TADF. No delayed emission was observed at 10 K, only the decay of phosphorescence after about 10 μs. For compound **3**, the enhancement of prompt fluorescence lifetime was observed at 10 K, indicating weaker non-radiative losses at 10 K. No TADF was observed at room temperature. Probably the weak TADF, observed in toluene solutions, was quenched in neat films with efficient exciton migration towards defect sites.

Optimization of exciplex TADF

The emergence of the dominating exciplex emission is shown in Fig. 9 a and b, where the fluorescence spectra of PMMA films doped with compound **1** at the concentration ranging from 1 to 100 wt% are demonstrated. Fluorescence peaked at about 460 nm at low doping concentration (0.1 – 2 wt%), where no intermolecular interactions were present, similarly as emission of $^1\text{CT}_1$ state in toluene. Some mismatch of emission energies were due to the different polarity of toluene and PMMA (toluene is more polar ambient) and presence of conformational disorder. Fluorescence peak started to redshift down to about 490 nm for the doping concentrations of 5 – 30 wt% due to the emergence and later increasing number of exciplex states. Almost no further redshift of emission spectra were observed at the larger doping concentrations (30 – 100 wt%), when the exciplex fluorescence clearly dominated.

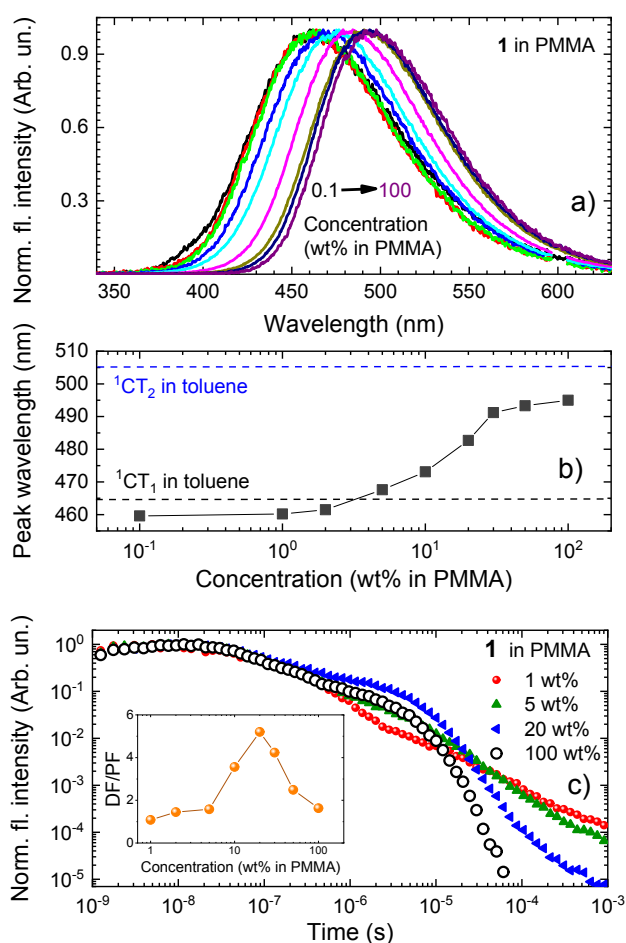


Fig. 9 a) Normalized time-integrated fluorescence spectra of compound **1** embedded in PMMA surrounding at different concentration. b) Fluorescence peak wavelengths of compound **1** embedded in PMMA surrounding at different concentration. c) Normalized fluorescence decay transients of compound **1** in PMMA at different doping concentrations. The inset shows DF/PF ratio at the different doping concentrations.

The transition from intramolecular TADF from to intermolecular TADF from exciplex states was also observed in fluorescence decay transients of compound **1** doped in PMMA at different concentrations (see Fig. 9 c). As we can see, fluorescence decay transients of 1 wt% and 5 wt% doped PMMA films were rather similar, when the emission of $^1\text{CT}_1$ states with the strong impact of conformation disorder dominates, however the rise of exciplex TADF is already observed at 5 wt% concentration. At the larger doping concentrations (e.g., 10 wt%), DF/PF ratio is enhanced (see the inset in Fig. 9), due to the emergence of the additional TADF from exciplex states²⁴. The DF/PF ratio peaks at about 20 wt% doping concentration and later starts to decrease at the larger doping loads, due to the enhanced excitation mobility and subsequent quenching of the latest delayed emission at the defect sites⁵¹ (see Fig. S10 in ESI). Such behavior was especially evident in the neat films. Similar trend was also observed for TADF lifetime, which tended to decrease at the larger doping concentration due to the quenching of the latest conformer states with the largest fluorescence lifetime.

As we can see, intermolecular TADF is unavoidable in heavily doped polymer films, however the DF/PF ratio can be enhanced by selecting the proper doping concentration.

Conclusions

In summary, we presented a comprehensive analysis of photophysical properties of series of donor- σ -acceptor TADF compounds with different donor units. Hyperconjugated hexafluoroisopropylidene spacer unit was selected to reduce the electronic communication between the donor and acceptor units seeking negligible singlet-triplet energy gap. However, to weak donor-acceptor coupling was observed, leading to remarkably prolonged fluorescence lifetime and allowing to observe several unusual effects. Firstly, the coexisting intra- and intermolecular fluorescence of different wavelength was observed at different time-scales even in solutions. Secondly, the initial decay with remarkably prolonged lifetime was shown to be simple prompt intramolecular CT fluorescence, which lifetime was lower for compounds with weaker electron-donating units. Interestingly, this slow initial fluorescence was susceptible to molecular oxygen. The later delayed fluorescence was shown to be TADF, originating from exciplex states, as proven by concentration and viscosity-dependent fluorescence measurements. In diluted polymer films with weakened non-radiative recombination, both prompt fluorescence and TADF were of intramolecular nature. Rather strong conformational disorder was observed due to flexible molecular structure, leading to large temporal shifts of emission peak. With an increasing doping load, a rise of exciplex TADF was observed, which dominated in neat films at similar wavelength as in solutions. However, the fractional intensity of TADF and its lifetime peaked at about 20 wt% doping concentration, since the further increase of doping load enabled the excitation migration towards the defect sites and subsequent quenching of the latest TADF.

Our results have shown that the weak coupling between donor and acceptor units is not favorable for the efficient intramolecular TADF in σ -bridged compounds and the hyperconjugated spacer unit should be carefully designed. In-line, intermolecular interactions should be minimized in order to prevent the exciplex emission in highly doped films.

Conflicts of interest

There are no conflicts of interest to declare.

Acknowledgements

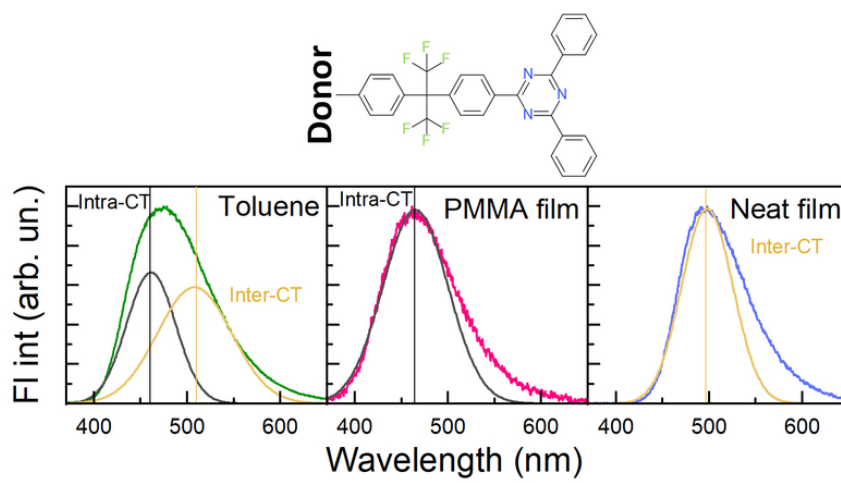
SJ and ChA acknowledge funding through the EU Marie Skłodowska-Curie ITN TADFlife grant (GA. 812872). ChA also acknowledges to Japan Science and Technology Agency (JST), ERATO, Adachi Molecular Exciton Engineering Project under JST ERATO Grant Number 436 JPMJER1305, and JSPS KAKENHI Grant Number 437 17H01232.

References

- 1 C. W. Tang and S. A. VanSlyke, *Appl. Phys. Lett.*, 1987, **51**, 913.
- 2 M. A. Baldo, D. F. O'Brien, Y. You, A. Shoustikov, S. Sibley, M. E. Thompson and S. R. Forrest, *Nature*, 1998, **395**, 151–154.
- 3 J.-H. Jou, S. Kumar, A. Agrawal, T.-H. Li and S. Sahoo, *J. Mater. Chem. C*, 2015, **3**, 2974–3002.
- 4 A. Endo, K. Sato, K. Yoshimura, T. Kai, A. Kawada, H. Miyazaki and C. Adachi, *Appl. Phys. Lett.*, 2011, **98**, 083302.
- 5 H. Uoyama, K. Goushi, K. Shizu, H. Nomura and C. Adachi, *Nature*, 2012, **492**, 234–238.
- 6 R. K. Konidena and J. Y. Lee, *Chem. Rec.*, 2018, **18**, 1-20.
- 7 M. Y. Wong and E. Zysman-Colman, *Adv. Mater.*, 2017, **29**, 1605444.
- 8 T. Hatakeyama, K. Shiren, K. Nakajima, S. Nomura, S. Nakatsuka, K. Kinoshita, J. Ni, Y. Ono and T. Ikuta, *Adv. Mater.*, 2016, **28**, 2777–2781.
- 9 M. Mamada, K. Inada, T. Komino, W. J. Potscavage, H. Nakanotani and C. Adachi, *ACS Cent. Sci.*, 2017, **3**, 769–777.
- 10 Y. Xu, X. Liang, X. Zhou, P. Yuan, J. Zhou, C. Wang, B. Li, D. Hu, X. Qiao, X. Jiang, L. Liu, S. Su, D. Ma and Y. Ma, *Adv. Mater.*, 2019, **31**, 1807388.
- 11 F. B. Dias, T. J. Penfold and A. P. Monkman, *Methods Appl. Fluor.*, 2017, **5**, 012001.
- 12 J. Gibson, A. P. Monkman and T. J. Penfold, *ChemPhysChem*, 2016, **17**, 2956–2961.
- 13 M. K. Etherington, J. Gibson, H. F. Higginbotham, T. J. Penfold and A. P. Monkman, *Nat. Commun.*, 2016, **7**, 13680.
- 14 K. Goushi, K. Yoshida, K. Sato and C. Adachi, *Nat. Phot.*, 2012, **6**, 253–258.
- 15 M. Colella, P. H. Pander, D. D. S. Pereira and A. P. Monkman, *ACS Appl. Mat. Interfaces*, 2018, **10**, 793–798.
- 16 M. Sarma and K.-T. Wong, *ACS Appl. Mat. Interfaces*, 2018, **10**, 19279–19304.
- 17 D. Chen, G. Xie, X. Cai, M. Liu, Y. Cao and S.-J. Su, *Adv. Mat.*, 2016, **28**, 239–244.
- 18 H. Tsujimoto, D.-G. Ha, G. Markopoulos, H. S. Chae, M. A. Baldo and T. M. Swager, *J. Am. Chem. Soc.*, 2017, **139**, 4894–4900.
- 19 K. Kawasumi, T. Wu, T. Zhu, H. S. Chae, T. Van Voorhis, M. A. Baldo and T. M. Swager, *J. Am. Chem. Soc.*, 2015, **137**, 11908–11911.

- 20 S. Shao, J. Hu, X. Wang, L. Wang, X. Jing and F. Wang, *J. Am. Chem. Soc.*, 2017, **139**, 17739–17742.
- 21 E. Spuling, N. Sharma, I. D. W. Samuel, E. Zysman-Colman and S. Bräse, *Chem. Commun.*, 2018, **54**, 9278–9281.
- 22 Y.-Z. Shi, K. Wang, X. Li, G.-L. Dai, W. Liu, K. Ke, M. Zhang, S.-L. Tao, C.-J. Zheng, X.-M. Ou and X.-H. Zhang, *Angew. Chem., Int. Ed.*, 2018, **57**, 9480–9484.
- 23 S.-Y. Qiu, H. Xu, L. Li, H.-T. Xu, L.-K. Meng, H.-S. Pang, C. Tang, Z.-Q. Pang, J. Xiao, X. Wang, S.-H. Ye, Q.-L. Fan and W. Huang, *J. Phys. Chem. C*, 2017, **121**, 9230–9241.
- 24 D. Zhang, K. Suzuki, X. Song, Y. Wada, S. Kubo, L. Duan and H. Kaji, *ACS Appl. Mat. Interfaces*, 2019, **11**, 7192–7198.
- 25 Y. Geng, A. D'Aleo, K. Inada, L.-S. Cui, J. U. Kim, H. Nakanotani and C. Adachi, *Angew. Chem., Int. Ed.*, 2017, **52**, 16763–16767.
- 26 P. L. dos Santos, J. S. Ward, D. G. Congrave, A. S. Batsanov, J. Eng, J. E. Stacey, T. J. Penfold, A. P. Monkman and M. R. Bryce, *Adv. Sci.*, 2018, **5**, 1700989.
- 27 M. Inoue, T. Serevičius, H. Nakanotani, K. Yoshida, T. Matsushima, S. Juršėnas and C. Adachi, *Chem. Phys. Lett.*, 2016, **644**, 62–67.
- 28 Z. Kuang, G. He, H. Song, X. Wang, Z. Hu, H. Sun, Y. Wan, Q. Guo and A. Xia, *Phys. Chem. C*, 2018, **122**, 3727–3737.
- 29 J. C. de Mello, H. F. Wittmann and R. H. Friend, *Adv. Mater.*, 1997, **9**, 230–232.
- 30 C. Rothe and A. P. Monkman, *Phys. Rev. B*, 2003, **68**, 075208.
- 31 Y. Im, M. Kim, Y. J. Cho, J.-A. Seo, K. S. Yook and J. Y. Lee, *Chem. of Mater.*, 2017, **29**, 1946–1963.
- 32 A. Köhler and H. Bässler, *Electronic processes in organic semiconductors: an introduction*, Wiley-VCH, Weinheim, 2015.
- 33 Y. Qu, P. Pander, A. Bucinskas, M. Vasylieva, Y. Tian, F. Miomandre, F. B. Dias, G. Clavier, P. Data and P. Audebert, *Chem. Eur. J.*, 2019, **25**, 2457–2462.
- 34 Y. Zhang, H. Ma, S. Wang, Z. Li, K. Ye, J. Zhang, Y. Liu, Q. Peng and Y. Wang, *J. Phys. Chem. C*, 2016, **120**, 19759–19767.
- 35 K. L. Woon, C.-L. Yi, K.-C. Pan, M. K. Etherington, C.-C. Wu, K.-T. Wong and A. P. Monkman, *J. Phys. Chem. C*, 2019, **123**, 12400–12410.
- 36 M. Sarma and K.-T. Wong, *ACS Appl. Mat. Interfaces*, 2018, **10**, 19279–19304.
- 37 P. Valat, V. Wintgens, Y. L. Chow and J. Kossanyi, *Can. J. Chem.*, 1995, **73**, 1902–1913.
- 38 S. A. Boer, R. P. Cox, M. J. Beards, H. Wang, W. A. Donald, T. D. M. Bell and D. R. Turner, *Chem. Commun.*, 2019, **55**, 663–666.
- 39 E. V. Bichenkova, A. R. Sardarian, A. N. Wilton, P. Bonnet, R. A. Bryce and K. T. Douglas, *Org. Biomol. Chem.*, 2006, **4**, 367–378.
- 40 T. C. Barros, S. Brochsztain, V. G. Toscano, P. B. Filho and M. J. Politi, *J. Photochem. Photobiol. A*, 1997, **111**, 97–104.
- 41 T. Serevičius, T. Bučiūnas, J. Bucevičius, J. Dodonova, S. Tumkevičius, K. Kazlauskas and S. Juršėnas, *J. Mater. Chem. C*, 2018, **6**, 11128–11136.
- 42 T. Northey, J. Stacey and T. J. Penfold, *J. Mat. Chem. C*, 2017, **5**, 11001–11009.
- 43 T. Serevičius, R. Skaisgiris, J. Dodonova, L. Jagintavičius, J. Bucevičius, K. Kazlauskas, S. Jursenas and S. Tumkevicius, *Chem. Commun.*, 2019, **55**, 1975–1978.
- 44 M. K. Etherington, F. Franchello, J. Gibson, T. Northey, J. Santos, J. S. Ward, H. F. Higginbotham, P. Data, A. Kurowska, P. L. Dos Santos, D. R. Graves, A. S. Batsanov, F. B. Dias, M. R. Bryce, T. J. Penfold and A. P. Monkman, *Nat. Commun.*, 2017, **8**, 14987.
- 45 X. Zhang, M. W. Cooper, Y. Zhang, C. Fuentes-Hernandez, S. Barlow, S. R. Marder and B. Kippelen, *ACS Appl. Mat. Interfaces*, 2019, **11**, 12693–12698.
- 46 T. Serevičius, R. Komskis, P. Adomėnas, O. Adomėnienė, G. Kreiza, V. Jankauskas, K. Kazlauskas, A. Miasojedovas, V. Jankus, A. P. Monkman and S. Jursenas, *J. Phys. Chem. C*, 2017, **121**, 8515–8524.
- 47 C. F. Madigan and V. Bulović, *Phys. Rev. Lett.*, 2003, **91**, 247403.

- 48 B. L. Cotts, D. G. McCarthy, R. Noriega, S. B. Penwell, M. Delor, D. D. Devore, S. Mukhopadhyay, T. S. De Vries and N. S. Ginsberg, *ACS Energy Lett.*, 2017, **2**, 1526–1533.
- 49 Q. Zhang, D. Tsang, H. Kuwabara, Y. Hatae, B. Li, T. Takahashi, S. Y. Lee, T. Yasuda and C. Adachi, *Adv. Mater.*, 2015, **27**, 2096–2100.
- 50 M. K. Etherington, N. A. Kukhta, H. F. Higginbotham, A. Danos, A. N. Bismillah, D. R. Graves, P. R. McGonigal, N. Haase, A. Morherr, A. S. Batsanov, C. Pflumm, V. Bhalla, M. R. Bryce and A. P. Monkman, *J. Phys. Chem. C*, 2019, **123**, 11109–11117.
- 51 M. Colella, A. Danos and A. P. Monkman, *J. Phys. Chem. Lett.*, 2019, **10**, 793–798.



77x43mm (300 x 300 DPI)